

FLOW-INDUCED VIBRATION OF A CIRCULAR CYLINDER AT LIMITING STRUCTURAL PARAMETERS

D. SHIELS, A. LEONARD AND A. ROSHKO

*Graduate Aeronautics Laboratories, California Institute of Technology
Pasadena, CA 91125, U.S.A.*

(Received 2 September 1998, and in final form 19 July 2000)

Transverse oscillation of a dynamically supported circular cylinder in a flow at $Re = 100$ has been numerically simulated using a high-resolution viscous-vortex method, for a range of dynamical parameters. At the limiting case with zero values of mass, damping and elastic force, the cylinder oscillates sinusoidally at amplitude $A/D = 0.47$ and frequency $fD/U_\infty = 0.156$. For zero damping, the effects of mass and elasticity are combined into a new, “effective” dynamic parameter, which is different from the classic “reduced velocity”. Over a range of this parameter, the response exhibits oscillations at amplitudes up to 0.6 and frequencies between 0.15 and 0.2. From this response function, the classic response in terms of reduced velocity can be obtained for fixed values of the cylinder/fluid ratio m^* . It displays “lock-in” at very high values of m^* .

© 2001 Academic Press

1. INTRODUCTION

THE FLOW-INDUCED VIBRATION of an elastically constrained two-dimensional circular cylinder has become a canonical problem in the efforts to understand more general situations of fluid–structure interactions. The situation in which vibration is permitted only transverse to the freestream (Figure 1) has received particular attention as a fundamental case. Relevant structural parameters are the system mass m (and associated density ρ_b), damping b , spring constant k , and diameter D . Important fluid parameters include the fluid density ρ , kinematic viscosity ν , and constant freestream velocity U_∞ . The cylinder is constrained to move only normal to the freestream; its transverse motion is determined by the lift generated from the flow. Vibration is thus governed by the equation of motion,

$$m \frac{d^2 y}{dt^2} + b \frac{dy}{dt} + ky = F_y, \quad (1)$$

where F_y is the instantaneous lift force and y is the transverse displacement.

Early studies such as the forced vibration experiments of Koopmann (1967) and the free vibration experiments of Feng (1968) established the viewpoint that the cylinder experiences significant vibration only when the characteristic shedding frequency nearly coincides with the natural structural frequency, $\omega_n = \sqrt{k/m}$, a state termed “lock-in”. Parkinson (1989) reviewed the various subsequent efforts to further define this lock-in behavior and to create models for the lift force, F_y , in equation (1) to facilitate prediction of the vibration characteristics of a given structure. These include the well-known proposal by Hartlen & Currie (1970). Other related reviews were given by Sarpkaya (1979) and Bearman (1984), and in a book by Blevins (1994). Griffin & Ramberg (1982) discussed the findings in the context of their application to practical problems.

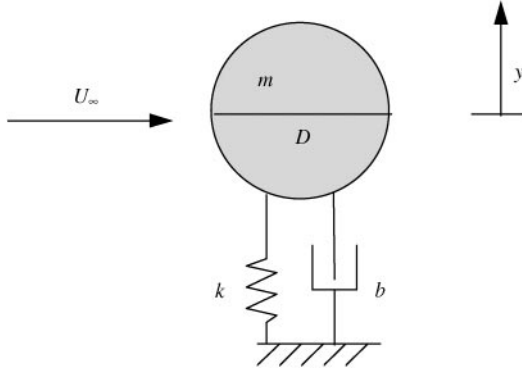


Figure 1. Problem under consideration.

Recent experimental results of Gharib *et al.* (1997), Gharib (1999) and Khalak & Williamson (1997) exhibited examples of significant flow-induced vibration without lock-in. On the other hand, classic lock-in was observed in the experiments of Brika & Laneville (1993) and Hover *et al.* (1997). The former experiments without lock-in were performed in water and were distinguished by low values of the mass ratio ρ_b/ρ while the latter experiments were performed in air, for which mass ratios are of order 10^3 . Thus, these various recent results suggest that the lock-in framework does not accurately describe the behavior of the system for all structural parameters, especially when the cylinder–fluid mass ratio becomes relatively small, as noted by earlier authors, e.g., Bearman (1984).

The simulations described in this paper explore limiting values for the structural parameters, m, b, k (each per unit span), in order to frame a more complete understanding of the system response. Traditionally, classification of the response has been based on utilization of the reciprocal of the mechanical frequency ω_n as a characteristic time. Thus, the freestream velocity is expressed as the reduced velocity, $U_R = U_\infty/\omega_n D$, and the nondimensional time $\tau = \omega_n t$. The equation of motion (1) can thus take on the relatively simple nondimensional form (using ω_n and D for nondimensionalization)

$$\frac{d^2 Y}{d\tau^2} + \zeta \frac{dY}{d\tau} + Y = c_y n U_R^2, \quad (2)$$

where $Y = y/D$, $\zeta = b/(2\sqrt{km})$ is the fraction of critical damping, $c_y = F_y/(\frac{1}{2}U_\infty^2 D)$ is the lift coefficient, and $n = \rho D^2/(2m)$ the mass parameter. On this basis, it has been the practice to scale results against U_R , n , and ζ , because observations of lock-in suggested that the mechanical frequency controls the response. Griffin & Ramberg (1982) showed that, based on experimental results, the limit as the so-called “mass-damping parameter, ζ/n , tends to zero might define the maximum amplitude of cylinder response. Discussions of this parameter may be found in papers by Sarpkaya (1978), Bearman (1984), and Khalak & Williamson (1997).

In limiting cases such as a massless ($m = 0$) or elastically unconstrained ($k = 0$) configuration, the mechanical frequency ω_n no longer has a meaningful definition. Furthermore, the recent studies which did not exhibit lock-in leave the universality of the scaling underlying (2) in doubt. Therefore, in order to provide a reduction valid for the entire space of structural parameters, we introduce an alternative nondimensionalization of equation (1) which avoids ω_n , namely

$$m^* \ddot{y}^* + b^* \dot{y}^* + k^* y^* = c_y(t^*), \quad (3)$$

where

$$y^* = \frac{y}{D}, \quad t^* = t \frac{U_\infty}{D}, \quad m^* = \frac{m}{\frac{1}{2}\rho D^2} = \frac{\pi \rho_b}{2 \rho}, \quad b^* = \frac{b}{\frac{1}{2}\rho U_\infty D}, \quad k^* = \frac{k}{\frac{1}{2}\rho U_\infty^2},$$

and (\cdot) indicates $d(\cdot)/dt^*$. Also, $c_y(t^*)$ is the usual nondimensional transverse force, per unit span, exerted on the body by the flow, from all pressure and viscous stresses, as defined just after equation (2).

The cylinder response $y^*(t^*)$ is then a function of the parameters m^* , b^* , k^* . A final parameter that can be expected to influence the response is the Reynolds number $\text{Re} = U_\infty D/\nu$, which sets the flow characteristics. All simulations presented in this study are at $\text{Re} = 100$.

2. COMPUTATIONAL METHOD

A viscous vortex method capable of achieving high resolution is used for computational simulation in this study. In addition to a cursory discussion of its basic features in Gharib (1999), the method is more thoroughly discussed in Shiels (1998). It has been extensively validated in the latter work, and in past studies such as that by Koumoutsakos & Leonard (1995).

Briefly, the two-dimensional vortex method tracks the evolution of the vorticity field governed by

$$\frac{D\omega}{Dt} = \nu \nabla^2 \omega \quad (4)$$

by creating elements of vorticity at the viscous cylinder boundary in order to satisfy the velocity boundary conditions and convecting those elements according to

$$\mathbf{u}(\mathbf{x}, t) = -\frac{1}{2\pi} \iint \frac{(\mathbf{x} - \mathbf{x}') \times \omega \hat{\mathbf{z}}}{|\mathbf{x} - \mathbf{x}'|^2} d\mathbf{x}' + \mathbf{U}_\infty \quad (5)$$

The particular vortex method used in this study includes viscous effects using the particle strength exchange method (Degond & Mas Gallic 1989; Komoutsakos & Leonard 1995).

At each step in the simulation, the transverse force coefficient $c_y(t^*)$ is obtained, then used to numerically integrate equation (3) and thus update the cylinder trajectory. As shown in Shiels (1998), the coefficient can be expressed in terms of the existing vorticity field and its normal derivative on the cylinder surface,

$$c_y = -\frac{1}{\text{Re}} \int_0^{2\pi} \left(\frac{1}{2} \frac{\partial \omega^*}{\partial r^*} - \omega^* \right) \cos \theta d\theta + \frac{\pi}{2} \dot{y}^*, \quad (6)$$

where $\theta = 0$ refers to the base of the cylinder (i.e. the downstream stagnation point in potential flow). All nondimensionalization can be assumed to use cylinder diameter and freestream velocity unless otherwise noted. In equation (6), the integral of the second term in brackets, which is seen to be proportional to the vorticity at the wall, gives the viscous contribution to c_y . The integral of the first term in brackets, the vorticity flux, plus the acceleration term gives the pressure contribution, calculated using the tangential component of the momentum equation at the boundary. The vorticity flux has two components, one due to the acceleration of the body and the other due to the motion of the vorticity already present in the boundary layer and wake. It is informative to consider how equation (6) can be used to treat an accelerating body in potential flow. In this case, the no-through flow

condition at the body surface is satisfied by a vortex sheet of variable strength $\gamma(\theta, t)$ along the surface of the body. Because the body has nonzero acceleration when it is oscillating, the sheet strength must be changing in time. The vorticity flux given by $-(1/\text{Re})(\partial\omega^*/\partial r^*)$ is equal to $(d\gamma^*/dt^*)$ and thus provides the necessary rate of change of sheet strength, independent of Re including $\text{Re} \rightarrow \infty$. The vorticity flux due to acceleration then gives $-\pi\ddot{y}^*$ as a contribution to c_y . Thus, for an accelerating body in a steady, inviscid freestream, one can obtain the apparent-mass force

$$c_{ya} = -(\pi/2)\ddot{y}. \quad (7)$$

Now it is important to note that in a viscous flow, body acceleration produces exactly the same contribution to the vorticity flux independent of Re , as mentioned above, but also independent of the vorticity field in the boundary layer and wake of the body. It is due to the excess pressure gradients around the body caused by the acceleration. For viscous flow, we therefore decompose the transverse force or ‘‘lift’’ coefficient as follows:

$$c_y(t) = c_{ya}(t) + c_{yw}(t) = -(\pi/2)\ddot{y}^*(t) + c_{yw}(t). \quad (8)$$

The ‘‘wake’’ lift term c_{yw} captures the frictional forces as well as altered pressure forces caused by the boundary layer and wake growth in viscous flow. In inviscid flow, with no boundary layer and wake, $c_{yw} = 0$. This lift decomposition is key to computation of the limiting case $m = 0, b = 0, k = 0$. For these structural parameters, the governing equation (3) becomes $c_y(t) = 0$ but a motion is still possible as the ‘‘wake’’ lift $c_{yw}(t)$ must balance the apparent-mass lift. In inviscid flow, no motion could be supported for $m = 0, b = 0, k = 0$ since $c_{yw}(t) = 0$. But in viscous flow, motion of the body generates a wake and induces a nonzero $c_{yw}(t)$ which in turn requires the body acceleration to provide $c_{ya}(t) = -c_{yw}(t)$. Various subtle issues concerning the numerical implementation of equation (6) in concert with equation (3) are discussed in Shiels (1998).

To assess the vortex method used in the present numerical simulation, a comparison is made in Table 1 with recent results from other numerical methods at the same value of $\text{Re} = 100$ for a stationary cylinder. Experimental results for an oscillating cylinder, over a range of low values of Re including $\text{Re} = 100$, were obtained by Anagnostopoulos & Bearman (1992). A comparison with their results is made later in this paper.

Results from the present numerical simulations for various combinations of the parameters (m^*, b^*, k^*) are listed in Tables 2 and 3.

3. RESULTS

3.1. MASSLESS ($m^* = 0$), UNDAMPED ($b^* = 0$) AND ELASTICALLY UNCONSTRAINED ($k^* = 0$) SIMULATION

The extreme limit on the mechanical part of the system is to essentially remove all of it, leaving only the requirement that the surface of the massless cylinder must remain solid.

TABLE 1
Comparison of results for stationary cylinder

| Reference | St | C_D | C_L |
|---------------------------|-------|-------|-------|
| Stansby & Slaouti (1993) | 0.166 | 1.32 | 0.35 |
| Anagnostopoulos (1994) | 0.167 | 1.20 | 0.27 |
| Henderson (1995) | 0.166 | 1.35 | 0.33 |
| Zhou <i>et al.</i> (1999) | 0.162 | 1.48 | 0.31 |
| Present | 0.167 | 1.33 | 0.30 |

TABLE 2
Results for $Re = 100$ simulations at zero damping ($b^* = 0$)

| k^* | m^* | k_{eff}^* | U_R | U_{RA} | A^* | f^* | C_L | C_{LW} | C_D |
|----------------|-------|--------------------|-------|----------|-------|-------|-------|----------|-------|
| 0 | 4 | -3.94 | | | 0.05 | 0.158 | -0.20 | -0.28 | 1.32 |
| 0 | 2.5 | -2.34 | | | 0.07 | 0.154 | -0.15 | -0.25 | 1.31 |
| 0 | 1.5 | -1.33 | | | 0.09 | 0.150 | -0.10 | -0.23 | 1.30 |
| 0 | 0.88 | -0.72 | | | 0.10 | 0.144 | -0.07 | -0.20 | 1.29 |
| 0 | 0.625 | -0.47 | | | 0.12 | 0.138 | -0.05 | -0.19 | 1.32 |
| 0 | 0.4 | -0.29 | | | 0.24 | 0.136 | -0.06 | -0.34 | 1.40 |
| 0 | 0.25 | -0.19 | | | 0.35 | 0.140 | -0.04 | -0.47 | 1.49 |
| 4.74 | 5 | -0.06 | 1.03 | 1.18 | 0.46 | 0.156 | 0.04 | -0.65 | 1.70 |
| 0 | 0 | 0.00 | | | 0.47 | 0.156 | 0.00 | -0.71 | 1.73 |
| 0.1 | 0.05 | 0.04 | 0.71 | 4.02 | 0.51 | 0.178 | 0.11 | -0.89 | 1.85 |
| 0.0707 | 0 | 0.07 | | 4.71 | 0.49 | 0.160 | 0.07 | -0.71 | 1.78 |
| 0.1414 | 0 | 0.14 | | 3.33 | 0.51 | 0.164 | 0.11 | -0.74 | 1.83 |
| 1 | 0.5 | 0.30 | 0.71 | 1.44 | 0.56 | 0.188 | 0.41 | -0.82 | 2.16 |
| 0.3535 | 0 | 0.35 | | 2.11 | 0.54 | 0.174 | 0.24 | -0.77 | 1.98 |
| 0.707 | 0 | 0.71 | | 1.49 | 0.57 | 0.184 | 0.45 | -0.75 | 2.16 |
| 2.48 | 1.25 | 0.74 | 0.71 | 1.07 | 0.57 | 0.188 | 0.48 | -0.76 | 2.19 |
| 4.96 | 2.5 | 1.17 | 0.71 | 0.91 | 0.58 | 0.196 | 0.77 | -0.60 | 2.22 |
| 8.74 | 5 | 1.31 | 0.76 | 0.87 | 0.57 | 0.194 | 0.83 | -0.50 | 2.26 |
| 1.414 | 0 | 1.41 | | 1.05 | 0.59 | 0.194 | 0.90 | -0.48 | 2.32 |
| 2 | 0 | 2.00 | | 0.89 | 0.58 | 0.200 | 1.22 | -0.22 | 2.32 |
| 9.88 | 5 | 2.14 | 0.71 | 0.82 | 0.57 | 0.198 | 1.35 | -0.02 | 2.23 |
| 2.31 | 0 | 2.31 | | 0.82 | 0.59 | 0.196 | 1.40 | 0.01 | 2.24 |
| 2.828 | 0 | 2.83 | | 0.75 | 0.57 | 0.189 | 1.70 | 0.55 | 2.13 |
| 3.5 | 0 | 3.50 | | 0.67 | 0.47 | 0.172 | 1.68 | 0.83 | 1.56 |
| 4 | 0 | 4.00 | | 0.63 | 0.39 | 0.184 | 1.60 | 0.78 | 1.64 |
| 14.84 | 7.5 | 4.38 | 0.71 | 0.78 | 0.34 | 0.188 | 1.52 | 0.77 | 1.42 |
| 4.5 | 0 | 4.50 | | 0.59 | 0.30 | 0.184 | 1.40 | 0.77 | 1.57 |
| 19.78 | 10 | 5.83 | 0.71 | 0.76 | 0.19 | 0.188 | 1.08 | 0.66 | 1.50 |
| 6 | 0 | 6.00 | | 0.51 | 0.14 | 0.182 | 0.85 | 0.56 | 1.43 |
| 8 | 0 | 8.00 | | 0.44 | 0.08 | 0.176 | 0.61 | 0.47 | 1.38 |
| 12 | 0 | 12.00 | | 0.36 | 0.04 | 0.172 | 0.48 | 0.41 | 1.36 |
| 29.68 | 15 | 12.97 | 0.71 | 0.75 | 0.06 | 0.168 | 0.55 | 0.44 | 1.35 |
| 16 | 0 | 16.00 | | 0.31 | 0.03 | 0.172 | 0.44 | 0.38 | 1.35 |
| Fixed cylinder | | | | | 0.00 | 0.167 | 0.30 | 0.30 | 1.33 |

TABLE 3
Results for $Re = 100$ simulations with $m^* = 0$ and $k^* = 2$

| b^* | A^* | f^* | C_L | ϕ (degrees) |
|--------|-------|-------|-------|------------------|
| 0 | 0.58 | 0.200 | 1.22 | -1.2 |
| 0.1675 | 0.55 | 0.194 | 1.15 | 4.5 |
| 0.5 | 0.48 | 0.192 | 1.04 | 15.6 |
| 1 | 0.39 | 0.190 | 0.93 | 28.7 |
| 2 | 0.25 | 0.182 | 0.79 | 46.6 |
| 3 | 0.18 | 0.180 | 0.70 | 57.3 |
| 4 | 0.12 | 0.176 | 0.63 | 63.2 |
| 8 | 0.06 | 0.172 | 0.50 | 73.8 |

This example is not only interesting in its own right but it is useful in displaying unambiguously the concept of apparent mass. Setting $m^* = 0$, $b^* = 0$, and $k^* = 0$ in equation (3) leaves the cylinder free to move in the transverse plane solely under the influence of forces which are induced by unsteady vorticity, without mechanical or inertial forces, yielding

$c_y = 0$. As discussed above, the motion of the cylinder in this situation is defined by balancing the forces generated by the wake development, c_{yw} , with the apparent mass term, $c_{ya} = -\frac{1}{2}\pi\ddot{y}^*$,

$$0 = c_y = c_{yw} + c_{ya} = c_{yw} - \frac{1}{2}\pi\ddot{y}^*. \quad (9)$$

Thus, the trajectory of the body $y^*(t^*)$ is up-dated at each time-step of the simulation based on the “wake force” c_{yw} .

In the simulation, the cylinder quickly reaches a periodic state in which it oscillates with an amplitude of nearly one radius ($A/D = 0.47$). Figure 2 indicates how quickly the periodic state is reached and that a single frequency ($f^* = 0.156$) dominates the response. A third harmonic is also present, though nearly undetectable.

The wake lift amplitude $c_{Lw} = 0.71$, which is found from the numerical computation [equation (6)], balances the apparent-mass term, which can be computed using equation (9),

$$\frac{1}{2}\pi\ddot{y}_{\max}^* = \frac{1}{2}\pi(4\pi^2 f^{*2} A^*) = \frac{1}{2}\pi(4\pi^2)(0.156)^2(0.47) = 0.709. \quad (10)$$

It is notable that the response frequency is not greatly different from the shedding frequency for a fixed cylinder in $Re = 100$ flow, namely $f^* = 0.165$, and the vorticity field established in the wake, shown in Figure 3, looks similar to the shedding pattern of a fixed cylinder.

Thus, without structural forces to influence response, the cylinder motion seems strongly drawn to a state defined by the natural characteristics of the wake. The wake is compliant enough to produce a periodic state fairly similar to its natural state, yet with important differences to support the motion of the cylinder.

Again, this example illustrates the meaning and definition of the apparent-mass force as the instantaneous inertial reaction of the fluid to acceleration of the cylinder; in fact, it is the same in a general, separated flow field as in potential flow, or in stationary fluid. Thus, with equation (8), equation (3) may be rewritten in the form

$$(m^* + \frac{1}{2}\pi)\ddot{y}^* + b^*\dot{y}^* + k^*y^* = c_{yw}(t^*). \quad (11)$$

3.2. MASSLESS ($m^* = 0$) AND UNDAMPED ($b^* = 0$) SIMULATIONS WITH NONZERO ELASTICITY

The system response in the absence of mechanical influences raises questions about the relation between that limiting state and classical lock-in behavior. To begin exploring this

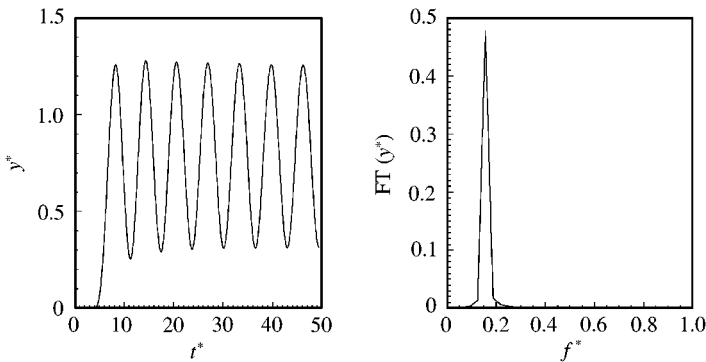


Figure 2. Transverse motion y^* and frequency spectrum of the cylinder response sampled over five cycles of periodic motion.

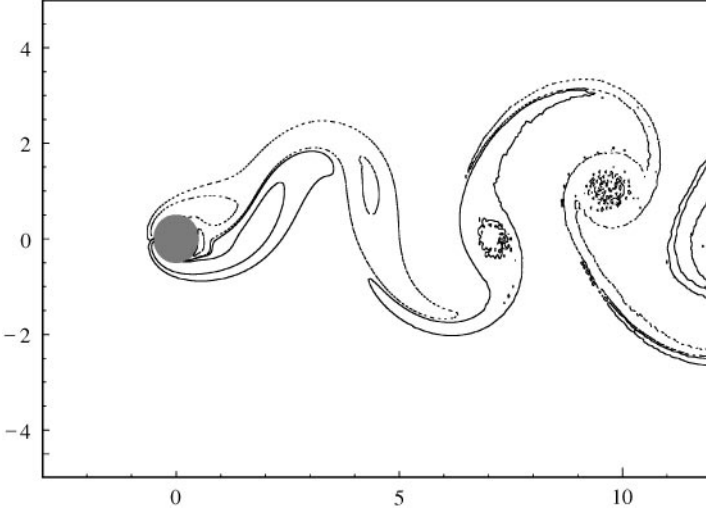


Figure 3. Vorticity field for $m^* = 0$, $b^* = 0$, $k^* = 0$ at minimum y^* . Contours at $\omega^* = \pm 0.2, \pm 2.0$.

issue, supports are considered in which only the elastic resistive force is included, i.e.,

$$\frac{1}{2}\pi \ddot{y}^* + k^* y^* = c_{yw}(t^*). \quad (12)$$

Simulation was possible only for $k^* > 0$; negative k^* led to unstable cylinder response. The results are listed in Table 2 and plotted in Figure 4. Examining equation (12), one might expect a strong response or resonance for $k^* \approx \frac{1}{2}\pi\omega^{*2}$. However, we see that it is only a little greater than at $k^* = 0$.

Sweeping over a range up to $k^* = 16$ did reveal, however, a sizeable region in which the cylinder exhibited a periodic response with large amplitude, $A^* \sim 0.5$. In this range ($0 < k^* < 3$), the response can be well defined by $y^* = A^* \sin(2\pi f^* t^*)$, where $A^* = A/D$, $f^* = fD/U_\infty$, the traditional response parameters. Beyond this, up to $k^* \approx 5$, there is a similar primary frequency of the cylinder response but amplitude modulation occurs as competing response frequencies become apparent, as in the example in Figure 5. For larger k^* , the response again becomes sinusoidal but with a greatly diminished amplitude.

As seen in Figure 4, the amplitude and frequency of the response increase slightly in the region $k^* < 3$. The response is nearly a pure sinusoid as in the $k^* = 0$ case. The drag also increases in this region. The large increase in the maximum lift from 0 to 2 is interesting in light of the fact that the cylinder motion is relatively constant as measured by the amplitude and frequency. At $k^* = 1.414$, the wake pictured in Figure 6 yields a fluctuating lift with amplitude $c_L = 0.9$ for a nearly sinusoidal motion defined by $A^* = 0.59$ and $f^* = 1.94$. At $k^* = 2.828$ (Figure 7), a similar nearly sinusoidal motion results with $A^* = 0.57$ and $f^* = 1.89$, but $c_L = 1.7$. The difference in c_L is notable but the striking difference is in the values of c_{Lw} , which are -0.48 and $+0.55$, respectively. The topology of the wake in these cases differs only a little from the $k^* = 0$ case, but still reveals a capacity in the flow to supply a broad range of lift while maintaining a classical shedding pattern. This is the classic 2S pattern (Williamson & Roshko 1988), i.e. two vortices (one of each sign) per shedding cycle.

The behavior observed for $k^* < 3$ is at odds with the conventional notion that such a high amplitude can occur only for the system near lock-in conditions (i.e. where the

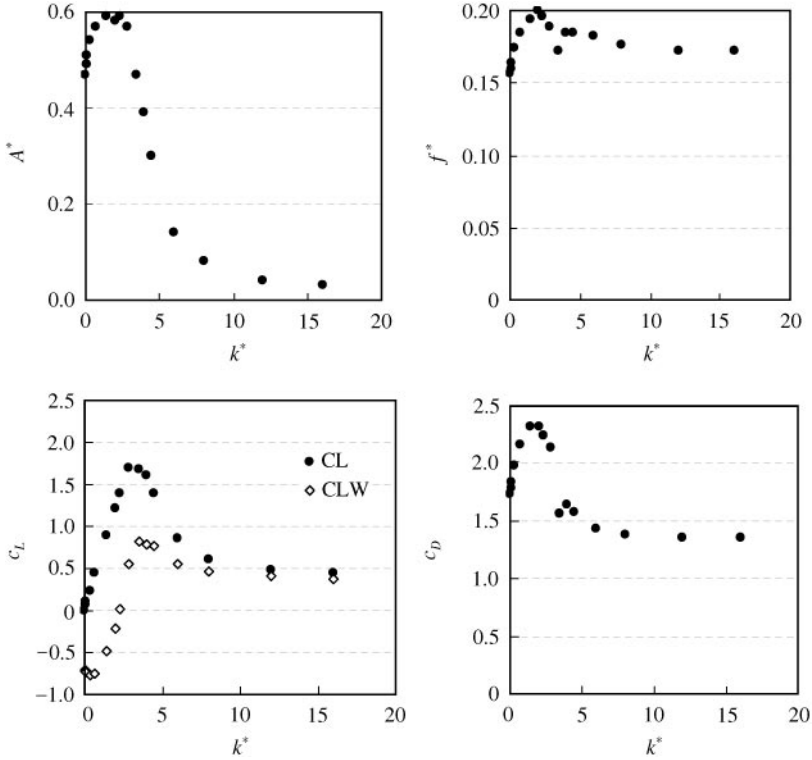


Figure 4. Results for $m^* = 0$, $b^* = 0$, $k^* \neq 0$: (a) amplitude A^* ; (b) frequency f^* ; (c) cross-force amplitude c_L ; (d) mean drag coefficient c_D .

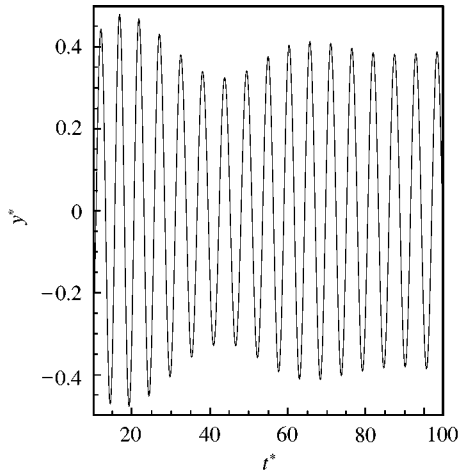


Figure 5. Cylinder response $y^*(t)$ for $m^* = 0$, $b^* = 0$, $k^* = 4$.

mechanical frequency lies close to the natural shedding frequency). In fact, such conditions are not even defined for a massless body.

As k^* increases beyond 3, the cylinder response begins to be modulated, as noted earlier. For such cases, the maximum value of the modulated response is shown in Figure 4; the

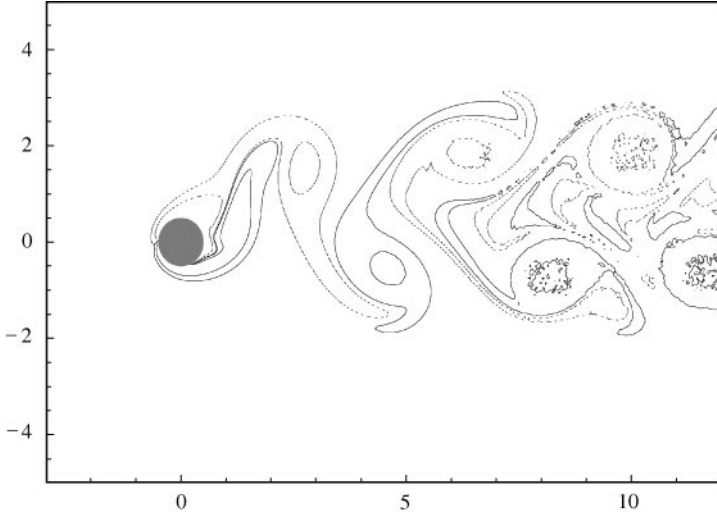


Figure 6. Vorticity field for $m^* = 0$, $b^* = 0$, $k^* = 1.414$ at minimum y^* . Contours at $\omega^* = \pm 0.2$, ± 2.0 ; $A^* = 0.59$, $f^* = 0.194$, $c_L = 0.90$, $c_D = 2.32$.

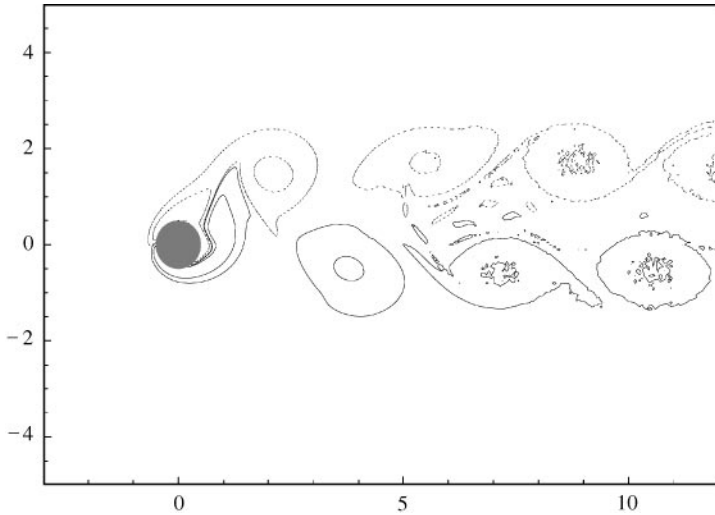


Figure 7. Vorticity field for $m^* = 0$, $b^* = 0$, $k^* = 2.828$ at minimum y^* . Contours at $\omega^* = \pm 0.2$, ± 2.0 ; $A^* = 0.57$, $f^* = 0.189$, $c_L = 1.70$, $c_D = 2.13$.

frequency shown is the primary one. However, simulations were only carried out for a time of 50–60 diameters of downstream motion, which often provided an incomplete view of the system response for these more complex motions. This perhaps explains why some data in the $3 < k^* < 5$ region seem to deviate from smooth trends in the frequency and drag.

As k^* becomes even larger, the parameters in Figure 4 can be seen decaying towards a fixed cylinder state ($A^* = 0$). The drag approaches asymptotically towards the fixed-cylinder mean value of $c_{D,avg} = 1.33$. Similarly, the lift amplitude decreases towards $c_L = 0.30$ and the frequency f^* approaches 0.165.

An interesting result occurs for the simulation with $k^* = 2.31$ (Figure 8), which is intermediate to the two cases ($k^* = 1.414$ and 2.828) discussed above and very close to the

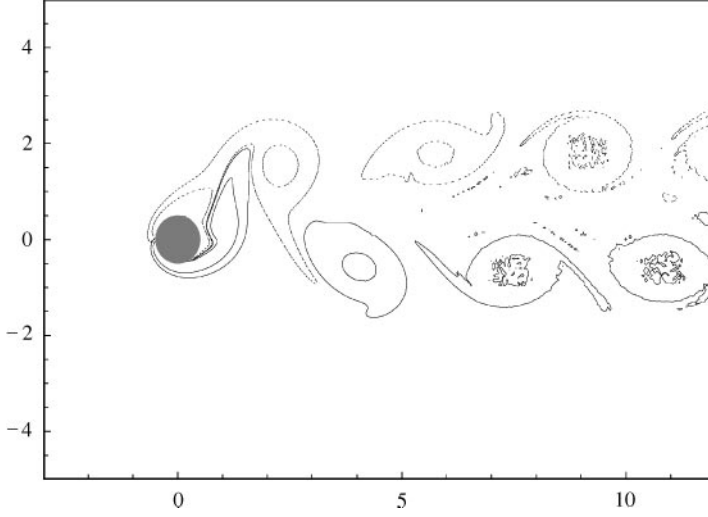


Figure 8. Vorticity field for $m^* = 0$, $b^* = 0$, $k^* = 2.31$ at minimum y^* . Contours at $\omega^* = \pm 0.2$, ± 2.0 ; $A^* = 0.59$, $f^* = 0.196$, $c_L = 1.40$ $c_D = 2.24$.

“resonance” condition $k^* \approx \frac{1}{2}\pi\omega^{*2}$. The amplitude is unchanged and the component of transverse force provided by the wake is now nearly zero ($c_{Lw} = 0.01$); the major component is from the apparent mass contribution. Figure 8 shows that there is no large, obvious change in the wake and it is not clear how adjustments are made so that the wake essentially makes no contribution to the lift at any time during its periodic motion. It is possible that small changes in the near-wake rotate the pressure distribution sufficiently to provide zero component of transverse force, $c_{y\omega}(t) = 0$. The streamwise force component would be only slightly affected (“cosine correction”); indeed, at this condition $c_D = 2.24$, which is typical for the higher amplitude motion (Table 2). At this particular value of k^* , the observed response frequency is almost exactly that defined by the mechanical system if the apparent mass is used to define a natural frequency for this $m^* = 0$ configuration:

$$f^*(k^* = 2.31) = 0.196 \approx f_{na}^* = \frac{1}{2\pi} \sqrt{\frac{k^*(=2.31)}{m_a^*(=\frac{1}{2}\pi)}} = 0.193 \quad (13)$$

This observation is developed further in the following sections.

3.3. UNDAMPED ($b^* = 0$) SIMULATIONS WITH NONZERO MASS AND ELASTICITY; EFFECTIVE k^*

Based on the observation that nearly pure sinusoidal motion occurs for $m^* = 0$, it is possible to predict the effects of including mass by assuming a sinusoidal response. If pure sinusoidal motion, $y^* = A^* \sin \omega^* t^*$, is assumed, then equation (3) with no damping ($b^* = 0$) becomes

$$(-\omega^{*2}m^* + k^*)A^* \sin \omega^* t^* = c_L \sin \omega^* t^*, \quad (14a)$$

or

$$k_{\text{eff}}^* A^* = c_L, \quad (14b)$$

where the effective elasticity, k_{eff}^* is defined by

$$k_{\text{eff}}^* = (k^* - 4\pi^2 f^{*2} m^*). \quad (14c)$$

It may be seen from equations (14) that, for any choices (k^*, m^*) which keep k_{eff}^* constant, a single response is consistent with the governing equation of motion. Thus, the influence of k^* and m^* can be folded into the single parameter k_{eff}^* , the “effective” spring constant which expresses the fact that for pure sinusoidal motion, at zero damping, the inertia of the body essentially acts in opposition to the resistive elastic force. The inertia can be considered to modify the elastic coefficient.

It is not clear *a priori* how well scaling with k_{eff}^* will define behavior in the regions with multiple significant frequencies (such as $3 < k^* < 5$ with $m^* = 0$). In order to assess the new idea of scaling by k_{eff}^* , simulations were run with nonzero body mass as well as nonzero elasticity but still with no damping. These results are compared in Figures 9 and 10 with those found for the zero inertia case ($m^* = 0$). Various choices were used for m^* , up to a maximum of $m^* = 15$ at which point the body is nearly 10 times as dense as the surrounding fluid. The results, listed in Table 2 and shown in Figures 9 and 10, show that k_{eff}^* does in fact collapse the two parameters, m^* and k^* , into one effective parameter which properly scales the undamped system. For large values of k_{eff}^* , the amplitude A^* decreases toward zero and the other response parameters approach the fixed-cylinder values. By setting $k^* = 0$ and $m^* \neq 0$, it was also possible to determine the behavior for $k_{\text{eff}}^* < 0$, showing that the response quickly drops off, tending asymptotically toward the fixed cylinder values. Thus, a picture is formed of the complete response (A^*, f^*) of the undamped system at $\text{Re} = 100$, with a region of k_{eff}^* in which the wake and mechanical system can synchronize to establish a large-amplitude, periodic response. Outside of this region,

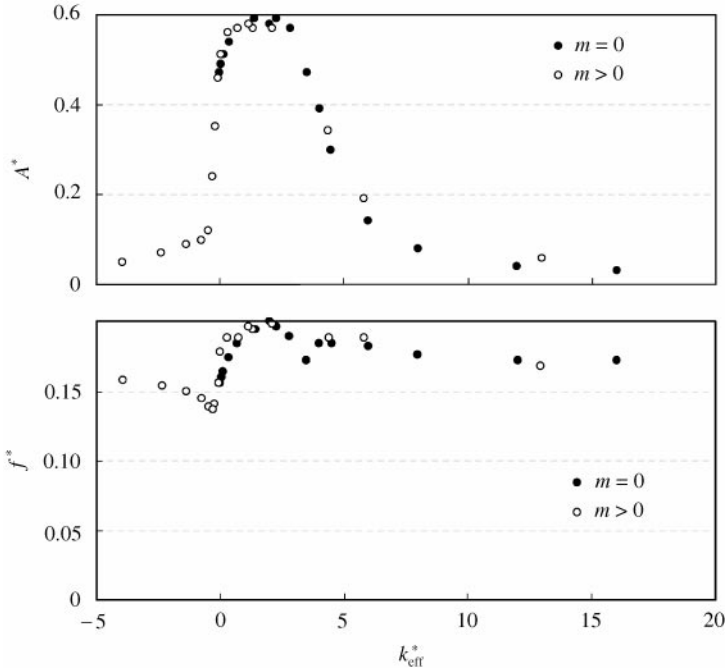


Figure 9. Response for undamped systems, with and without inertia, plotted against the effective elasticity: (a) amplitude A^* ; (b) frequency f^* : ●.

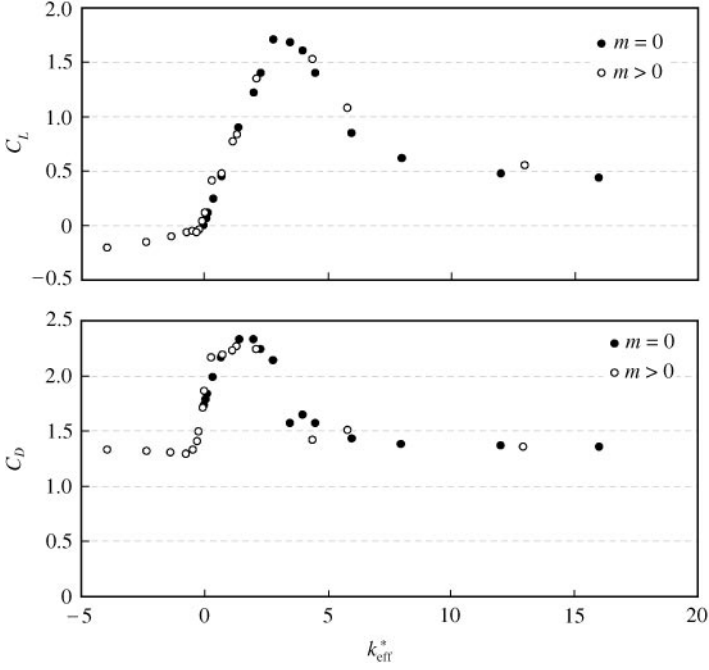


Figure 10. Lift amplitude and drag coefficient, plotted against effective elasticity. (Negative values of lift amplitude indicate that phase = π with respect to cylinder position.): ●.

significant motion of the body does not occur. Apparently, large motions cannot generate a wake to supply the required lift for these values of k_{eff}^* .

This effective elastic coefficient k_{eff}^* also provides a unified scaling for system behavior, provided it is dominated by a single frequency. Traditionally, the reduced velocity U_R has been invoked for scaling due to the perceived dependence of the system response on the natural mechanical frequency. However, the reduced velocity is undefined for cases where the elasticity or inertia is zero. The flaws in reduced velocity scaling are further evident by comparing it to scaling by k_{eff}^* on systems intentionally chosen to yield a constant reduced velocity but having different values of m^* . As seen in Figure 11(a), despite the fact that the reduced velocity is constant, a range of system responses are possible. Using $U_{R,a}$ equation (16) is not sufficient either as seen in Figure 11(c). Rather, these responses can be clearly defined through scaling by the effective elastic coefficient k_{eff}^* , as seen in Figure 11(b). Although the reduced velocity scaling proves deficient for a study where structural properties are varied, it is convenient when a constant mechanical frequency is simply used to nondimensionalize a variable freestream velocity.

3.4. REDUCED-VELOCITY SCALING; LOCK-IN

For $\text{Re} = 100$ and zero damping, the response of the cylinder, f^* and A^* , is given in Figures 9 and 10, and in Table 2, as functions of the effective elasticity k_{eff}^* . While these functions have been computed from a limited set of values of m^* and k^* , they describe, in principle, the response for all values, including values at which “lock-in” should be observed. To see the connection between our results and the traditional description, we proceed as follows. From equation (14c)

$$k_{\text{eff}}^* = k^* - \omega^{*2} m^* = m^*(\omega_n^{*2} - \omega^{*2}), \quad (15a)$$

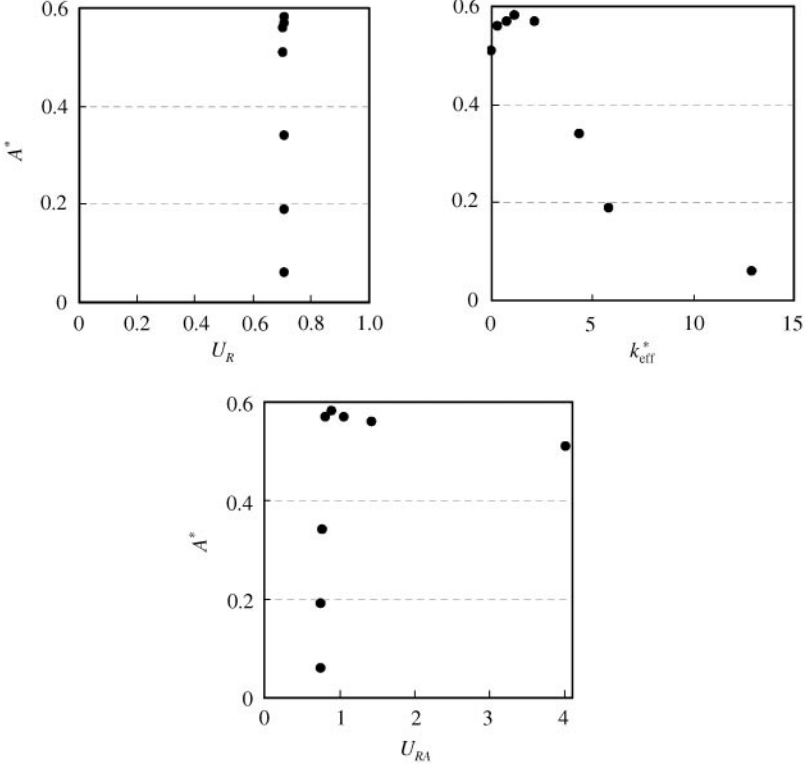


Figure 11. Selected results for $m \neq 0$; amplitude A^* versus (a) reduced velocity U_R , (b) effective elasticity k_{eff}^* , (c) reduced with apparent mass U_{RA} .

where

$$\omega_n^{*2} = U_R^{-2} = k^*/m^*, \quad (15b)$$

thus

$$\omega_n^{*2} = \omega^*{}^2 + k_{\text{eff}}^*/m^*. \quad (15c)$$

For a fixed value of m^* , each value of k_{eff}^* gives values of $\omega^* = 2\pi f^*$ and A^* from Table 2 or Figures 9 and 10, and thus a value of ω_n^* from equation (15c). This defines values of $U_R = 1/\omega_n^*$ and $f/f_n = \omega^*/\omega_n^*$, so that A^* and f/f_n can then be plotted in the traditional way. An example obtained for $m^* = 5$ is shown in Figure 12(a). The three values for $m^* = 5$, which were actually obtained from the simulation (Table 2), are also shown. Part of a second curve for $m^* = 20$ is also shown, in Figure 12(b). Traditionally, lock-in is understood as the tendency for the cylinder to oscillate at its “natural”, mechanical frequency, f_n , in some range of the dimensionless (“reduced”) velocity U_R , while keeping the mass ratio m^* constant. The tendency to lock-in as m^* increases is evident. Both these curves cross the axis $f/f_n = 1$ at $U_R \approx 1.02$. This must be the pivot point for every m^* , because it is the value corresponding to $k_{\text{eff}}^* = 0$ [see equation (15a)]. Thus, the solution for $m^* = 0$, $k^* = 0$ is also at this point, and we can infer that the corresponding “natural” frequency is, in some limiting sense, $f_n^* = f^* = 0.156$ (Table 2), which corresponds to $U_R = (2\pi f^*)^{-1} \approx 1.02$. Curves for $m^* < 5$ depart further from “lock-in”, but always pass through $U_R \approx 1.02$. The response for $m^* \rightarrow 0$ goes through that point, and $m^* = 0$ is singular in this plot.

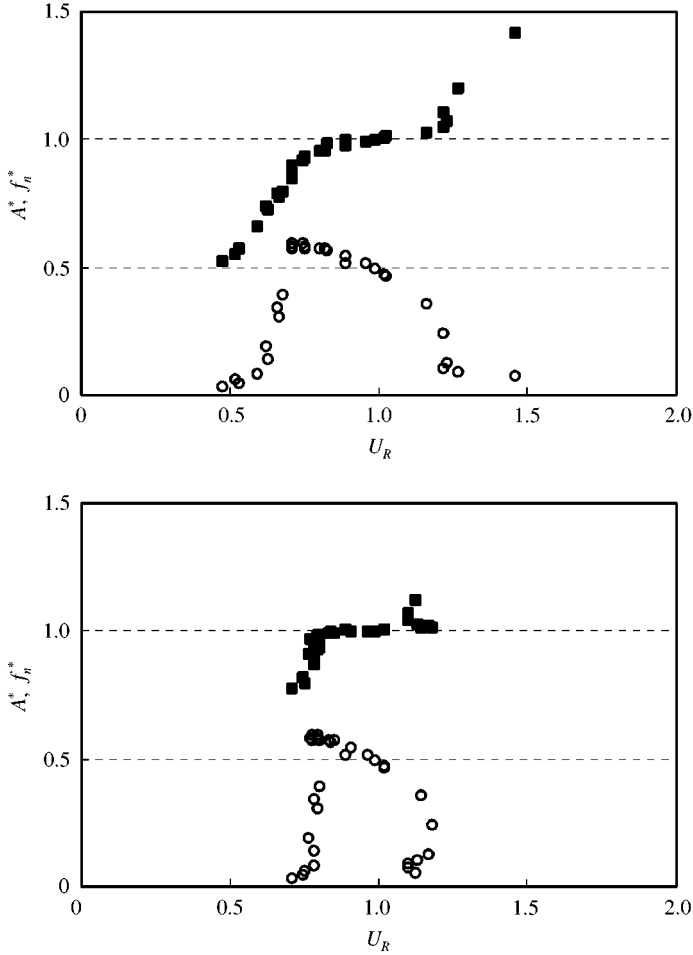


Figure 12. “Mapped” response plotted against reduced velocity, U_R : (a) $m^* = 5$, (b) $m^* = 20$: \circ , A^* ; \blacksquare , f^*/f_n^* .

The possibility of carrying out the inversion accurately for even higher values of m^* is limited by the precision of the values of f^* in Figure 9, because $\omega_n^* \rightarrow \omega^*$ asymptotically for $m^* \rightarrow \infty$, as may be seen from equations (15). For $m^* \gg 1$, equation (15c) may be approximated by

$$\omega^* - \omega_n^* \sim k_{\text{eff}}^*/2m^* \quad (15d)$$

(assuming $\omega^* \sim 1$ in the region of interest). Therefore, the precision needed for ω^* ($= 2\pi f^*$) is of the order $0.01 k_{\text{eff}}^*/m^*$.

At this point it is interesting to make a comparison of our results with the experimental measurements of Anagnostopoulos & Bearman (1992), which extended over a Reynolds-number range $90 < \text{Re} < 150$ as the reduced velocity ranged over $0.82 < U_R < 1.3$. The values of mass ratio ($n = 0.00427$) and damping ($\zeta = 0.00120$) in their experiment correspond to $m^* = 213$ and $b^* = 0.51$. Because of precision limitations noted above, it is difficult to map our k_{eff}^* coordinate onto U_R . Nevertheless, useful comparison is possible. First, with regard to frequency response, equation (15d) shows that in our high-amplitude range

($0 < k_e^* < 3$) the mapping will give $1 \leq \omega^*/\omega_n^* < 1.007$; indeed, the corresponding data of Anagnostopoulos & Bearman shows the frequency “locked in”.

The more interesting result concerns the amplitude A^* . Our model predicts the exact point of resonance ($\omega^* = \omega_n$) to occur at $k_{\text{eff}}^* = 0$ or $U_R = 1.02$ (for $\text{Re} = 100$). In Figure 2 of Anagnostopoulos & Bearman, the condition $U_R (= U_\infty/2\pi f_n D) = 1.02$ shows $A^* = 0.48$; this compares well to our value $A^* = 0.47$, perhaps surprisingly because their value of Re at this velocity is $\text{Re} = 115$. Their maximum value of $A^* = 0.55$, which occurs at ($U_R = 0.97$, $\text{Re} = 109$) may be compared with our maximum value, $A^* = 0.59$ at $k_{\text{eff}}^* = 2.31$, but the correspondence of the latter with U_R cannot be computed accurately, as noted. This limited comparison, with uncertainties about the effects of $\text{Re} = 100$ for the numerically simulated results, and with a free end on the cylinder, the possibility of slant shedding and finite, though small damping in the experimental results, is nevertheless encouraging!

3.5. SCALING PARAMETERS BASED ON APPARENT MASS

The data in Table 2 can be recalculated in terms of a mechanical frequency and corresponding reduced velocity that includes the apparent mass $m_a^* = \frac{1}{2}\pi$, i.e.,

$$\omega_{na}^{*2} = k^*/(m^* + \frac{1}{2}\pi) = (U_{R,a})^{-2}. \quad (16)$$

This makes it possible to better display the limiting case $m^* = 0$, for which

$$f_{na}^* = 2\pi(k^*/m_a^*)^{1/2} = 2\sqrt{2\pi k^*}.$$

The results for several values of m^* , including $m^* = 0$, are shown in Figure 13(a–f). For $m^* = 0$ we have an extreme departure from the lock-in line while a lock-in trend becomes apparent for $m^* \geq 5$. This is the tendency that may be seen in the results of Khalak & Williamson (1997) and of Gharib (1999). For very large values of m^* the curves will of course converge to those on the traditional plot of Figure 12. Again, for large values of m^* , the scatter connected with imprecision in the basic data for k_{eff}^* becomes apparent.

3.6. EFFECTS OF DAMPING

The idealization of zero damping provided a simplified system in which basic analysis could help to define the system response on terms of a single parameter. The addition of damping complicates matters because the single-frequency assumption does not simplify the equation of motion to the same extent. Due to the damping, a phase shift must be incorporated between the lift and body response. Consider as before a single-frequency response,

$$y^* = A^* \sin(2\pi f^* t^*), \quad (17)$$

and assume the lift behaves as

$$c_y = c_L \sin(2\pi f^* t^* + \phi). \quad (18)$$

Substitution into the equation of motion (3) yields two equations:

$$\frac{c_L}{A^*} = \sqrt{k_{\text{eff}}^{*2} + 4\pi^2 f^{*2} b^{*2}}, \quad (19a)$$

$$\phi = \tan^{-1} \left(\frac{2\pi f^* b^*}{k_{\text{eff}}^*} \right). \quad (19b)$$

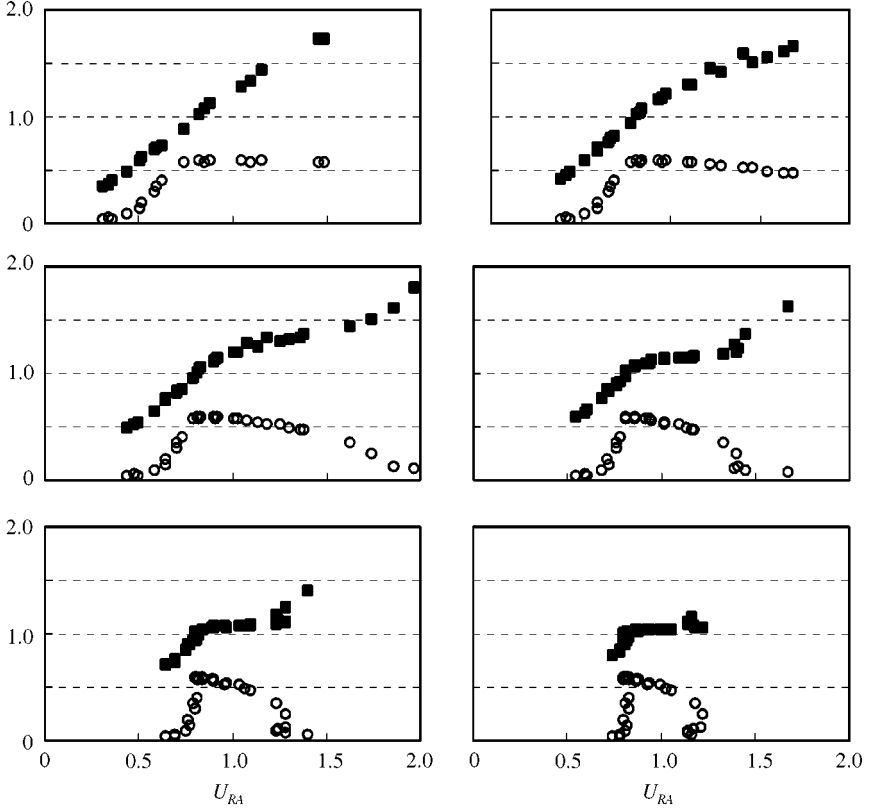


Figure 13. “Mapped” response plotted against reduced velocity, U_{RA} , with apparent mass included in the dynamics: (a) $m^* = 0$; (b) $m^* = 1$, (c) $m^* = 2$, (d) $m^* = 5$, (e) $m^* = 10$, (f) $m^* = 20$: \circ , A^* ; \blacksquare , $f_{m_a}^*$.

Thus, for constant damping, b^* , the parameter k_{eff}^* does define the system response wherever the single-frequency assumption is reasonable. Note, though, that at a given Reynolds number there could still be many families of responses as the required synchronization between the wake and body changes with b^* . Thus, the high-amplitude region for $b^* = 0$ studied above might not reflect the behavior at larger b^* . From an analytic perspective, both parameters are required to define the response of a damped system at a given Reynolds number.

In the current study, a few cases were simulated with fixed $m^* = 0$ and $k^* = 2$ in which damping was varied to get an idea of its effects. The results, shown in Figure 14 and tabulated in Table 3, were as expected. Damping tends to mute the amplitude response and the phase ϕ increases with larger damping (as the damping term thus comes to dominate the elastic term in the equation of motion). The frequency of response does not vary significantly, with higher frequency accompanying larger amplitude motion as observed in the undamped systems.

In linear vibration theory and in classical discussions of flow-induced vibration [equation (2)], the damping is represented by the nondimensional parameter $\zeta/b(4mk)^{-1/2}$. For low values of m , it seems appropriate to generalize it to include the apparent mass, i.e., $\zeta_a = b[4(m + m_a)k]^{-1/2}$, as was done by Khalak & Williamson (1997). The relation between the damping parameters, ζ_a and b^* , is

$$\zeta_a = b^*[4(m^* + \frac{1}{2}\pi)k^*]^{-1/2}. \quad (20)$$

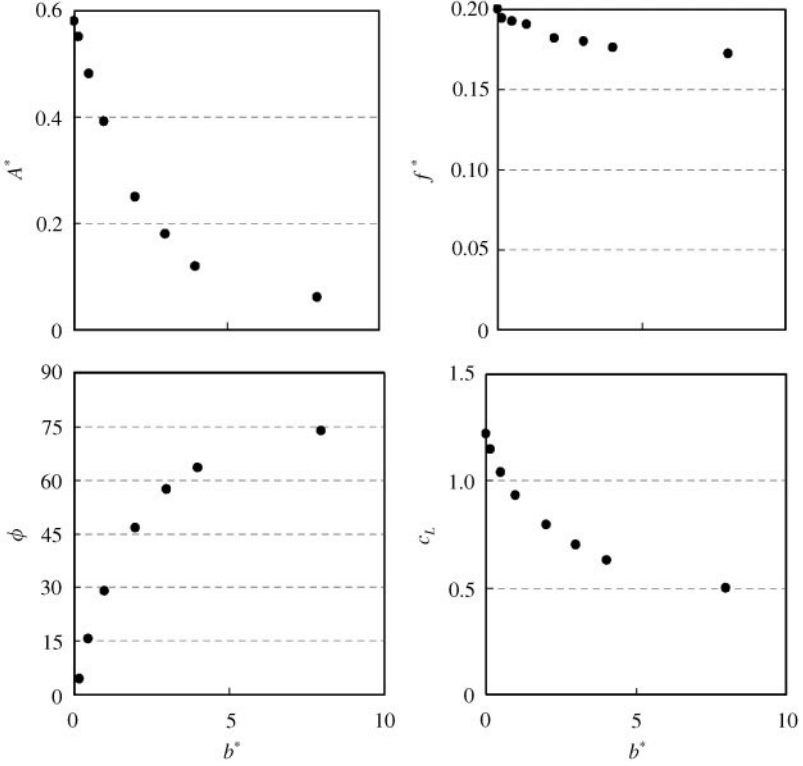


Figure 14. Response for damped systems with $m^* = 0, k^* = 2$: (a) amplitude A^* , (b) frequency f^* , (c) phase ϕ , (d) cross-force amplitude c_L .

For the example the computation described above, in which $m^* = 0, k^* = 2$, equation (20) gives $\zeta_a = b^*/2\sqrt{\pi} = 0.28b^*$.

The values of b^* (and correspondingly of ζ) used in our simulated example are large, compared to typical values in lightly damped systems, e.g., $\zeta = 0.0012$, in the experiments of Anagnostopoulos & Bearman (1992). Our limited example suggests that such low values of damping have negligible effect on the motion at low values of m^* . Interpolation of the data in Figure 14 and Table 3 indicates that, for a 1% decrease in amplitude A^* in the high-response regime, the damping needed is $b^* = 0.032$ or $\zeta_a = 0.009$ at $m^* \rightarrow 0$. However, for large values of m^* , a small value of ζ can result in a significant value of $b^* = 2(m^*k^*)^{1/2}\zeta = 2m^*\zeta/U_R$. It can be seen that our intrinsic damping parameter b^* is in fact the mass damping parameter $\zeta/n = \zeta m^*$, mentioned in the Introduction. (The factor $2/U_R \doteq 2$ since $U_R \sim 1$ in the response range.)

4. CONCLUDING DISCUSSION

There are several results worth noting. One is the finding that flow-induced “vibration” of a cylinder in cross-flow can occur at significant amplitudes even if there is no coupling to a mechanical system with which it might have a resonance. This is strikingly illustrated by the example of a cylinder with zero values of mass, damping and spring force, i.e. a cylinder free to move unconstrained in the cross-flow direction. With no definable mechanical

frequency, the classical “lock-in” scenario does not apply. Nevertheless, the cylinder oscillates, sinusoidally, with frequency and amplitude determined by a balance between the wake-vortex force and its own inertial (apparent-mass) reaction. The body motion and the trajectories of vorticity in the boundary layers and wake adjust to each other to continuously produce the necessary zero net crossforce on the body.

Adding mass m^* and spring force k^* to the system introduces two new parameters but, if damping is zero and the cylinder is sinusoidal, the inertial and elastic forces oppose each other and so can be combined into a single “effective” dimensionless parameter k_{eff}^* . Our and others’ explorations of the effects of damping suggest that a damping coefficient smaller than 10^{-2} has little effect on the motion especially at low values of m^* . Therefore, for lightly damped systems, it can be omitted, and the single parameter k_{eff}^* then completely defines the system at a given value of Reynolds number.

Another result concerns the relation of k_{eff}^* to “lock-in” which is loosely understood as a coincidence between the actual cylinder frequency $\omega^* = 2\pi f^* D/U_\infty$ and the frequency $\omega_n^* = \omega_n D/U_\infty$ of the mechanical system. But the coincidence occurs at only one value of the effective elasticity, $k_{\text{eff}}^* = k^* - \omega^{*2} m^* = m^*(\omega_n^{*2} - \omega^{*2})$, namely $k_{\text{eff}}^* = 0$. The motion is then identical to that at $m^* = 0$, $k^* = 0$, and the transverse force $C_L = 0$. This is true for any pair of values of m^* , k^* , even massive ones. While this is the only point at which frequencies coincide, large-amplitude motion occurs over a range given, approximately, by $0 < k_{\text{eff}}^* < 3$. The corresponding range for ω^* is given by

$$\omega_n^{*2} \leq \omega^{*2} \leq \omega_n^{*2} + 3/m^*.$$

It may be seen that, for large m^* , $\omega^* \simeq \omega_n^*$, in this range (the traditional lock-in range) but for $m^* \rightarrow 0$, the ratio of the two frequencies is strongly variable and traditional “lock-in” does not occur.

ACKNOWLEDGEMENTS

Thanks to Dr Mohammad Gharib and Prof. Morteza Gharib for their involvement throughout this research effort. This work has been supported by ONR Grant #N00014-94-1-0793. Computing time was partially provided by the JPL Supercomputing Project (funded from the NASA Offices of Mission to Planet Earth, Aeronautics, and Space Sciences). Scholarship support was provided under DoD Grant #DAAH04-93-G-0281.

REFERENCES

- ANAGNOSTOPOULOS, P. & BEARMAN, P. W. 1992 Response characteristics of a vortex-shedding cylinder at low Reynolds numbers. *Journal of Fluids and Structures* **6**, 39–50.
- ANAGNOSTOPOULOS, P. 1994 Numerical investigation of response and wake characteristics of a vortex-excited cylinder in a uniform stream. *Journal of Fluids and Structures* **8**, 367–390.
- BEARMAN, P. W. 1984 Vortex shedding from oscillating bluff bodies. *Annual Review of Fluid Mechanics* **16**, 195–222.
- BLACKBURN, H. & HENDERSON, R. 1996 Lock-in behavior in simulated vortex-induced vibration. *Experimental Thermal and Fluid Science* **12**, 184–189.
- BLEVINS, R. D. 1994 *Flow Induced Vibration, 2nd edition*. Malabar, FL: Krieger Publishing.
- BRIKA, D. & LANEVILLE, A. 1993 Vortex-induced vibrations of a long flexible circular cylinder. *Journal of Fluid Mechanics* **250**, 481–508.
- DEGOND, P. & MAS GALLIC, S. 1989 The weighted particle method for convection–diffusion equations. *Mathematics of Computation* **53**, 485–507.
- FENG, C. C. 1968 The measurement of vortex-induced effects in flow past stationary and oscillating circular and D-section cylinders. M.A.Sc. Thesis, University of British Columbia, Vancouver, B. C., Canada.

- GHARIB, M. R., SHIELS, D., GHARIB, M., LEONARD, A. & ROSHKO, A. 1997 Exploration of flow-induced vibration at low mass and damping. In *Proceedings of fourth International Symposium on Fluid-Structure Interaction, Aeroelasticity, Flow-Induced Vibration, and Noise* (eds M. P. Paidoussis *et al.*) Vo. 1, pp. 75–81. New York: ASME.
- GHARIB, M. R. 1999 Vortex-induced vibration absence of lock-in and fluid Force deduction. Ph.D. Thesis, California Institute of Technology, Pasadena, CA.
- GRIFFIN, O. M. & RAMBERG, S. E. 1982 Some recent studies of vortex shedding with application to marine tubulars and risers. *ASME Journal of Energy Research and Technology* **104**, 2–13.
- HARTLEN, R. T. & CURRIE, I. G. 1970 Lift-oscillator model of vortex-induced vibration. *ASCE Journal of Engineering Mechanics Division* **96**, 577–591.
- HENDERSON, R.D. 1995 Details of the drag curve near the onset of vortex shedding. *Physics of Fluids* **7**, 2102–2104. (Also, private communication.)
- HOVER, F.S., MILLER, S.N. & TRIANTAFYLLOU, M.S. 1997 Vortex-induced vibration of marine cables: experiments using force feedback. *Journal of Fluids and Structures* **11**, 307–326.
- KHALAK, A. & WILLIAMSON, C. H. K. 1997 Fluid forces and dynamics of a hydroelastic structure with very low mass and damping. *Journal of Fluids and Structures* **11**, 973–982.
- KOOPMANN, G. H. 1967 The vortex wakes of vibrating cylinders at low Reynolds numbers. *Journal of Fluid Mechanics* **28**, 501–512.
- KOUMOUTSAKOS, P. & LEONARD, A. 1995 High-resolution simulations of the flow around an impulsively started cylinder using vortex methods. *Journal of Fluid Mechanics* **296**, 1–38.
- PARKINSON, G. 1989 Phenomena and modelling of flow-induced vibrations of bluff bodies. *Progress in Aerospace Sciences* **26**, 169–224.
- SARPKAYA, T. 1979 Vortex-induced oscillations-a selective review. *Journal of Applied Mechanics* **46**, 241–258.
- SARPKAYA, T. 1978 Fluid forces on oscillating cylinders. *ASCE Journal of Waterways, Port, Coastal and Ocean Engineering* **104**, 275–290.
- SHIELS, D. 1998 Simulation of controlled bluff body flow with a viscous vortex method. Ph.D. Thesis, California Institute of Technology, Pasadena, CA.
- STANSBY, P. K. & SLAOUTI, A. 1993 Simulation of vortex shedding including blockage by the random-vortex and other methods. *International Journal for Numerical Methods in Fluids* **17**, 1003–1013.
- WILLIAMSON, C.H.K. & ROSHKO, A. 1988 Vortex formation in the wake of an oscillating cylinder. *Journal of Fluids and Structures* **2**, 355–381.
- ZHOU, C.V., SO R.M.C. & LAM, K. 1999 Vortex induced vibrations of an elastic circular cylinder. *Journal of Fluids and Structures* **13**, 165–189.